

Article

Numerical Investigation for the Resin Filling Behavior during Ultraviolet Nanoimprint Lithography of Subwavelength Moth-Eye Nanostructure

Yuanchi Cui ^{1,2}, Xuewen Wang ^{1,2}, Chengpeng Zhang ^{1,3,4,*}, Jilai Wang ^{1,2} and Zhenyu Shi ¹

- ¹ Key Laboratory of High Efficiency and Clean Mechanical Manufacture of Ministry of Education, School of Mechanical Engineering, National Demonstration Center for Experimental Mechanical Engineering Education, Shandong University, Jinan 250061, China; cuiyuanchi@mail.sdu.edu (Y.C.); xwwang1990@mail.sdu.edu (X.W.); jlwang@sdu.edu.cn (J.W.); shizhenyu@sdu.edu.cn (Z.S.)
- ² Nanjing Rolling Intelligent Manufacturing Research Institute, Nanjing Mumuxili Technology Co., Ltd., Nanjing 211100, China
- ³ State Key Laboratory of Mechanical System and Vibration, Shanghai Jiao Tong University, Shanghai 200240, China
- ⁴ Suzhou Institute of Shandong University, Shandong University, Suzhou 215123, China
- * Correspondence: zhangchengpeng@sdu.edu.cn

Abstract: Accurate analysis of the resin filling process into the mold cavity is necessary for the high-precision fabrication of moth-eye nanostructure using the ultraviolet nanoimprint lithography (UV-NIL) technique. In this research, a computational fluid dynamics (CFD) simulation model was proposed to reveal resin filling behavior, in which the effect of boundary slip was considered. By comparison with the experimental results, a good consistency was found, indicating that the simulation model could be used to analyze the resin filling behavior. Based on the proposed model, the effects of process parameters on resin filling behavior were analyzed, including resin viscosity, inlet velocity and resin thickness. It was found that the inlet velocity showed a more significant effect on filling height than the resin viscosity and thickness. Besides, the effects of boundary conditions on resin filling behavior were investigated, and it was found the boundary slip had a significant influence on resin filling behavior, and excellent filling results were obtained with a larger slip velocity on the mold side. This research could provide guidance for a more comprehensive understanding of the resin filling behavior during UV-NIL of subwavelength moth-eye nanostructure.

Keywords: CFD simulation; ultraviolet nanoimprint lithography; filling behavior; moth-eye nanostructure



Citation: Cui, Y.; Wang, X.; Zhang, C.; Wang, J.; Shi, Z. Numerical Investigation for the Resin Filling Behavior during Ultraviolet Nanoimprint Lithography of Subwavelength Moth-Eye Nanostructure. *Coatings* **2021**, *11*, 799. <https://doi.org/10.3390/coatings11070799>

Received: 30 May 2021

Accepted: 22 June 2021

Published: 1 July 2021

Publisher's Note: MDPI stays neutral with regard to jurisdictional claims in published maps and institutional affiliations.



Copyright: © 2021 by the authors. Licensee MDPI, Basel, Switzerland. This article is an open access article distributed under the terms and conditions of the Creative Commons Attribution (CC BY) license (<https://creativecommons.org/licenses/by/4.0/>).

1. Introduction

The moth-eye nanostructure has been widely used to reduce the surface reflection on optoelectronic products, such as liquid crystal display (LCD) [1,2], solar cell [3,4], image sensor [5], etc. Inspired by nature, the moth-eye nanostructure is a nipple array, typically of nano-scale height and diameter [6]. Its antireflection performance is closely related to structural accuracy, and therefore high-precision fabrication of moth-eye nanostructure is critical [7]. Among various fabrication technologies, the ultraviolet nanoimprint lithography (UV-NIL) provides an effective solution for the high-precision fabrication of moth-eye nanostructure [8,9], which mainly includes liquid resin filling into the mold cavity and UV-curing process. The filling process is core during UV-NIL of moth-eye nanostructure, which determines the final forming accuracy, so an accurate analysis of the resin filling behavior is necessary [10,11]. However, the moth-eye nanostructure is generally tens to hundreds of nanometers [12,13], and it is quite difficult to analyze the resin filling behavior through the experimental method. Therefore, numerical simulation is commonly adopted to investigate the resin filling behavior in micro/nano-scale [14,15].

Various researches have been carried out to investigate the resin filling behavior in the UV-NIL process. Kim et al. [16] studied the effects of contact angle and aspect ratio on the resin filling behavior, and it was found that complete filling occurred when the contact angle on the vertical wall was as low as that on the substrate. Lai et al. [17,18] investigated the effects of process parameters on bubble defects during roll-to-roll ultraviolet nanoimprint lithography (R2R UV-NIL) of the micro-pyramid array. Tian et al. [19] proposed a simulation model to predict the electrically induced pattern formation, which considered the effects of electrostatic force-assisted and electrocapillary force-driven. Nagaoka et al. [20] studied the resin filling characteristics under a condensable gas ambient, and it was found the gas ambient had a significant impact on the resin filling behavior. Shibata et al. [21] established a simulation system to investigate the UV-NIL process, which was composed of the resin filling module, optical-intensity distribution module, mechanical properties module and shrinkage module. Ye et al. [22] analyzed the generation mechanism of bubble defects in the R2R UV-NIL process.

Although various researches have been reported to analyze resin filling behavior, the moth-eye nanostructure is generally tens to hundreds of nanometers and boundary slip has a significant effect on the filling behavior at this scale [23,24]. Few simulation studies have been reported considering the effect of boundary slip. The computational fluid dynamics (CFD) simulation is an effective method to predict the behavior of liquids and gases in an intelligent way, which is widely used in aerospace, automotive, energy and other fields. Therefore, a CFD simulation model was proposed in this paper, which considered the effect of boundary slip. Based on the proposed model, the effects of process parameters and boundary conditions on resin filling behavior were investigated. Besides, the simulation results were also compared with experimental results, and good agreement was found. This research could provide guidance for the accurate analysis of resin filling behavior during UV-NIL of moth-eye nanostructure.

2. Numerical Modeling

2.1. Physical Model

Figure 1a shows the schematic diagram of resin filling process during UV-NIL of moth-eye nanostructure, where v is flow velocity of the resin, d the diameter of moth-eye nanostructure, h the height of moth-eye nanostructure and L the resin thickness. The imprinting mold for moth-eye nanostructure is 90 nm in diameter and 180 nm in depth, as shown in Figure 1b. A simulation model was built to investigate the resin filling behavior during UV-NIL of moth-eye nanostructure using the commercial program, ANSYS-Fluent, and the following assumptions were made to simplify the simulation process.

- (1) As shown in Figure 1b, the moth-eye nanostructure was rotationally symmetric, and therefore the simulation model was simplified to a two-dimensional model.
- (2) The resin filling process was assumed as an incompressible steady laminar flow during UV-NIL of moth-eye nanostructure [16,25].
- (3) The resin was assumed as an incompressible Newton fluid [20,26].
- (4) It was assumed that the resin flowed into the gap between the mold and substrate from one side at a certain speed and out from the other side [25].

2.2. Material Parameters

The material parameters could obviously affect filling behavior, so an accurate setting of material parameters in the simulation model was necessary. Two kinds of materials were included in the simulation model, that was air and resin. As one common material, the material parameters for air were chosen from a database in ANSYS-Fluent software (R15.0). The resin for fabrication of moth-eye nanostructure was a radical curing system developed by Jiangsu Kangde Xin Composite Material Co., Ltd. (Suzhou, China) [7,27] and its material parameters were obtained through experimental characterization, including viscosity, surface tension and wettability.

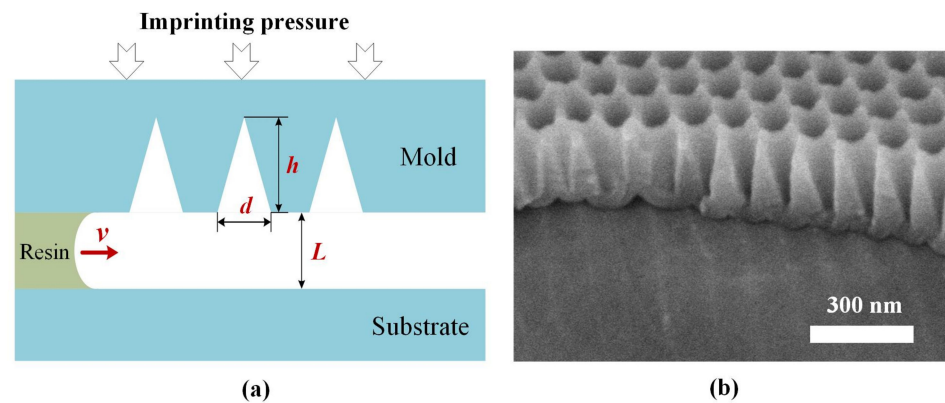


Figure 1. The UV-NIL of moth-eye nanostructure (a) schematic diagram (b) imprinting mold.

Figure 2 presented the viscosity property at different temperatures, which was obtained using the rotary viscometer (DV2T, Brookfield, Middleboro, MA, USA). It was found that the resin viscosity decreased as the temperature increased. When the temperature was raised from 25 °C to 65 °C, the resin viscosity was reduced from 322.3 mPa·s to 45.6 mPa·s. This phenomenon could be attributed to the thermal motion energy of polymer molecules that was larger with a higher temperature, which made the liquid internal pores increase in both number and volume, so the resin fluidity was better [18].

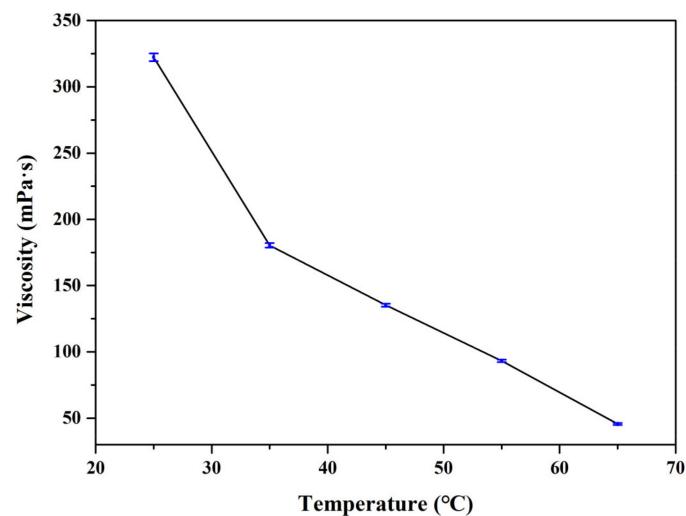


Figure 2. The resin viscosity at different temperatures.

Figure 3 displayed the surface tension at different temperatures, which was obtained with a surface tension tester (K100, Kruss, Hamburg, Germany) and Wilhelmy method. The temperature was set as 25 °C, 50 °C, 75 °C, respectively. As shown in Figure 3, the surface tension varied from 29.0 mN/m to 25.0 mN/m as the temperature was raised from 25 °C to 75 °C. The reason for this phenomenon was that the thermal motion became more intense inside the liquid, and the distance between molecules increased when the temperature rose, which caused the gravitational pull from the surface molecules to decrease accordingly. Moreover, the density of the gas phase and the gas stress relative to the surface molecules increased when the temperature rose. The two effects worked together, which caused surface tension to decrease at high temperatures [17].

Figure 4 gave the contact angle measurements, which were obtained using the contact angle measuring instrument (DSA30, Kruss, Hamburg, Germany). The volume of the droplet for contact angle measurements was 3 μ L. In order to ensure accuracy, at least five different positions were chosen to measure the contact angle on each sample surface, and the average of all measurements was taken as the contact angle of the sample surface.

Based on the measurements, the contact angle between resin with mold and polyethylene terephthalate (PET) substrate was $21.5 \pm 1.8^\circ$ and $28.3 \pm 2.1^\circ$, respectively.

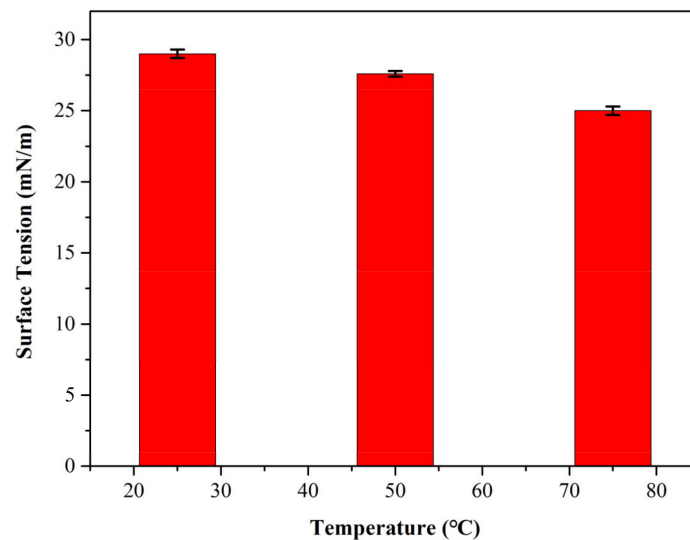


Figure 3. The surface tension of the resin at different temperatures.

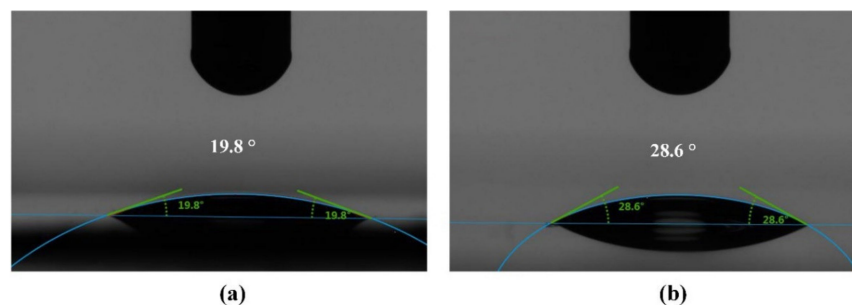


Figure 4. The contact angle between the resin and (a) mold (b) substrate.

Based on the experimental characterization above, the parameters in the simulation model were set as Table 1.

Table 1. Physical parameters in the filling simulation model.

Physical Constant	Values
Viscosity of the resin	0.05–0.35 Pa·s
Density of the resin	1200 kg/m ³
Viscosity of the air	1.79×10^{-5} Pa·s
Density of the air	1.225 kg/m ³
Surface tension of the resin	25–29 mN/m
Contact angle between the resin and substrate	$28.3 \times 2.1^\circ$
Contact angle between the resin and mold	$21.5 \times 1.8^\circ$

2.3. Boundary Conditions

Figure 5 presented the boundary conditions in the simulation model. As shown in Figure 1a, the resin flowed into the gap between the mold and substrate from one side at a certain speed and out from the other side. Therefore, the left side was considered to be the resin inlet, and the boundary condition was set as velocity inlet. The right side was considered to be the resin outlet, and the boundary condition was set as outflow. The top side was the impermeable mold surface, and the boundary condition was set as a wall. The bottom side was impermeable PET substrate, and the boundary condition was set as a wall.

According to whether the slip occurred, the wall boundary condition could be further set as no-slip wall and slip wall.

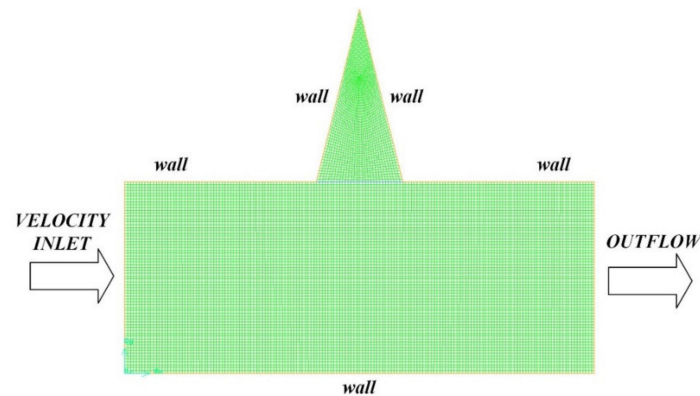


Figure 5. Boundary conditions in the simulation model.

2.4. Mathematic Equations

The Navier–Stokes equation was used to describe the resin flow behavior. Mass conservation was given by

$$\frac{\partial u}{\partial x} + \frac{\partial v}{\partial y} = 0 \quad (1)$$

where u was the velocity in x direction and v was the velocity in y direction.

Momentum conservation was given by

$$\rho \left(u \frac{\partial u}{\partial x} + v \frac{\partial u}{\partial y} \right) = -\frac{\partial p}{\partial x} + \mu \left(\frac{\partial^2 u}{\partial x^2} + \frac{\partial^2 u}{\partial y^2} \right) \quad (2)$$

$$\rho \left(u \frac{\partial v}{\partial x} + v \frac{\partial v}{\partial y} \right) = -\frac{\partial p}{\partial y} + \mu \left(\frac{\partial^2 v}{\partial x^2} + \frac{\partial^2 v}{\partial y^2} \right) \quad (3)$$

where p was the pressure, ρ the fluid density and μ the fluid viscosity.

In the simulation model, the air was set as the primary phase, and the resin was set as the secondary phase. The volume of fluid (VOF) method was employed to track the interface between resin and air [28,29]. The VOF function $f_{i,j}$ was defined in the entire flow field, which was the ratio of fluid volume to mesh volume in each mesh. A mesh that did not contain this fluid was called an empty mesh, a mesh that was filled with such a fluid was called a full mesh, and a mesh that contained an interface was called a half mesh. Assuming the calculation area was Ω and the fluid area was Ω_l , the following function was defined:

$$f(x, t) = \begin{cases} 1 & x \in \Omega_l \\ 0 & x \notin \Omega_l \end{cases} \quad (4)$$

The equation $\frac{\partial f(x,t)}{\partial t} + u \frac{\partial f(x,t)}{\partial x} + v \frac{\partial f(x,t)}{\partial y} = 0$ was satisfied in the flow field, and $V = (u, v)$ was the velocity field. The VOF function $f_{i,j}$ was defined as an integral of $f(x, t)$ on each mesh $I_{i,j}$.

$$f_{i,j} = \frac{1}{\Delta V_{i,j}} \int f(x, t) dV \quad (5)$$

The mesh with $f_{i,j} = 1$ was full of fluid, the mesh with $f_{i,j} = 0$ was called the empty mesh and the mesh with $0 < f_{i,j} < 1$ was called the boundary mesh. According to the $f_{i,j}$ value, the interface could be constructed.

2.5. Evaluation Method

The filling height was adopted to describe the simulation results quantitatively, as shown in Figure 6. After the filling process was completed, the simulation results were post-

processed, and then the resin volume fraction in the mold cavity was derived. According to the cloud image of volume fraction, the interface between resin and air could be extracted. In this research, the height value at the mold center line was defined as filling height.

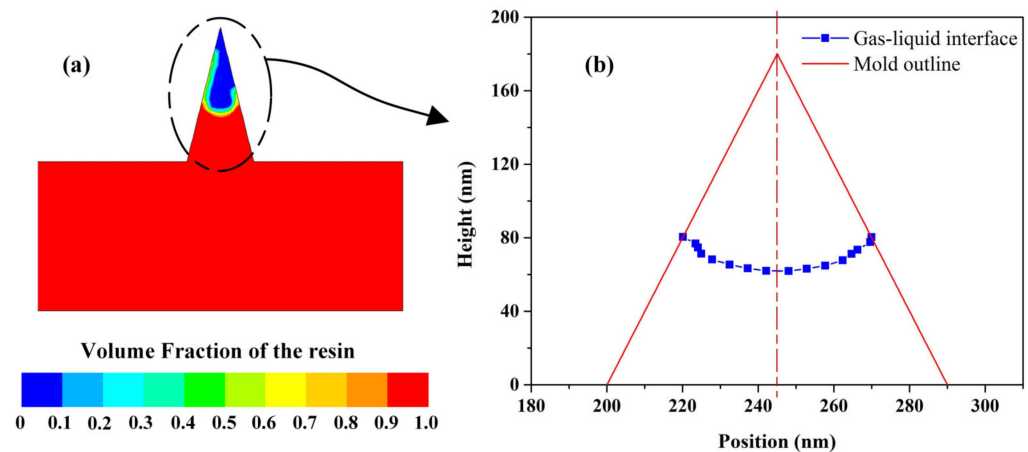


Figure 6. The filling height of moth-eye nanostructure from the simulation results. (a) the resin volume fraction in the mold cavity, (b) the interface between resin and air.

3. Results and Discussion

3.1. Effect of Process Parameters

Figure 7 showed the effect of resin viscosity on the filling height of the moth-eye nanostructure. In order to ensure one single variable, the inlet velocity and resin thickness were set as 1×10^{-5} m/s and 200 nm. As observed, the filling height decreased as the resin viscosity increased both with no-slip and slip boundaries. The reason for this phenomenon was that as the resin viscosity increased, the viscous resistance increased and less resin flowed into the mold cavity under the same conditions, thereby obtaining a lower filling height. Figure 8 displayed the moth-eye nanostructures fabricated by the UV-NIL process, and geometric characterization was conducted using atomic force microscope (AFM) equipment (Dimension FastScan, Bruker, Karlsruhe, Germany). As presented in Figure 8c, the forming height was acquired through bearing analysis of AFM images. It could be found that the simulation results with slip boundary were more compatible with the experimental results. The experimental results were slightly lower than the simulation heights, which might be caused by the curing shrink of the resin [30,31]. Based on the contrast between simulation and experimental results, the proposed simulation model considering the effect of boundary slip showed high accuracy, which could be used for the analysis of resin filling behavior during the UV-NIL of moth-eye nanostructure.

Figure 9 showed the effect of inlet velocity on the filling height of the moth-eye nanostructure. According to the simulation results, the filling height declined as the inlet velocity increased. It could be attributed to the mold cavity that was closed more quickly as the inlet velocity increased so that the resin volume flowing into the mold cavity decreased, eventually causing the height to decrease. Further analysis showed that a larger filling height could be obtained with slip boundary, which was because the resin near the mold side flowed faster than the substrate side, and more resin could be filled into the mold cavity before the cavity was closed. However, when the inlet velocity was larger than 7×10^{-5} m/s, the filling height was almost the same with both slip and no-slip boundaries. This was because the filling height was affected by the boundary and initial condition simultaneously. When the initial inlet velocity became larger, the influence of boundary slip was weakened, and the final height was mainly affected by the inlet velocity [32,33].

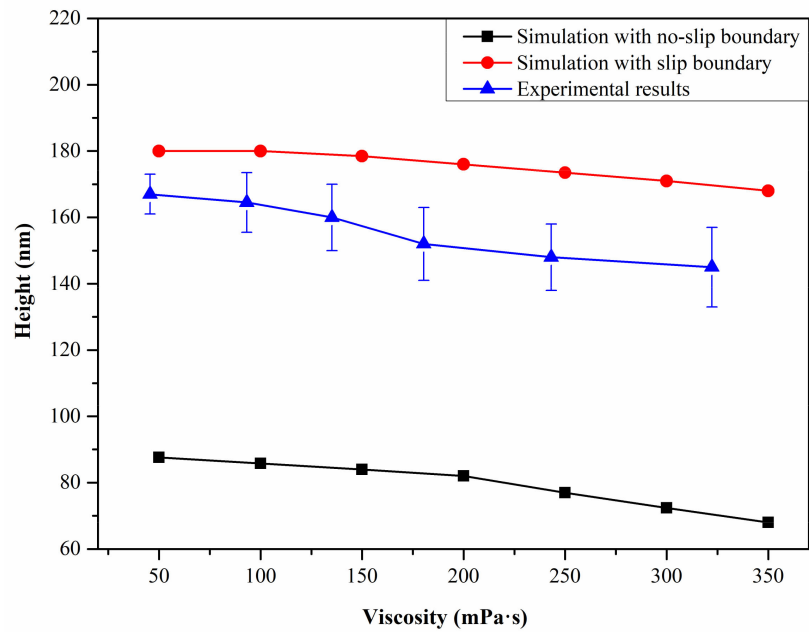


Figure 7. Effect of resin viscosity on the filling height of moth-eye nanostructure.

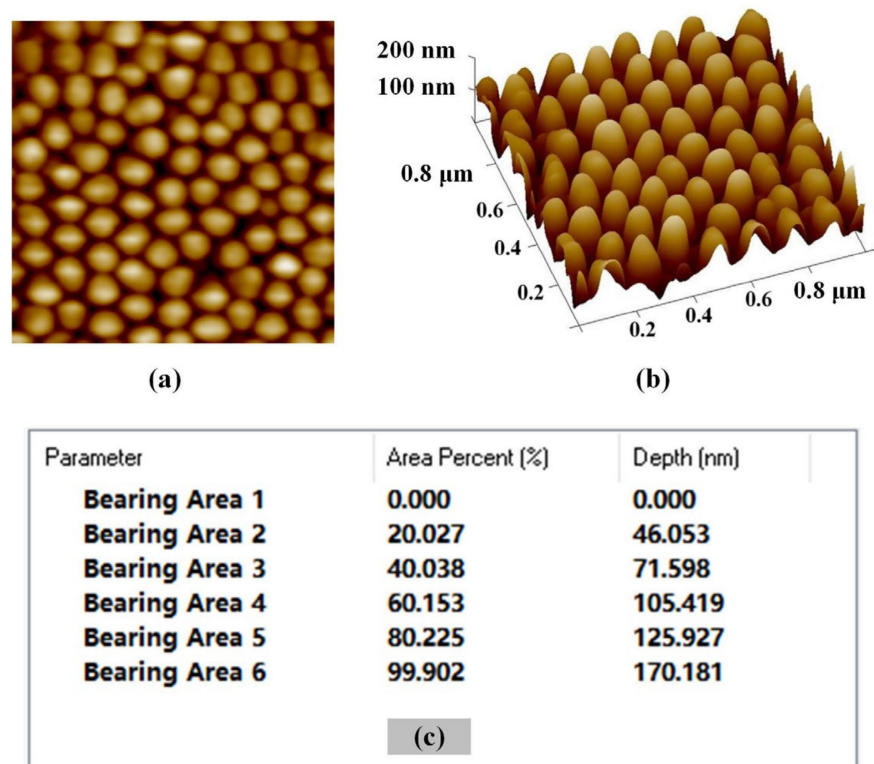


Figure 8. AFM characterization of the fabricated moth-eye nanostructure (a) two-dimensional topography (b) three-dimensional morphology (c) bearing analysis.

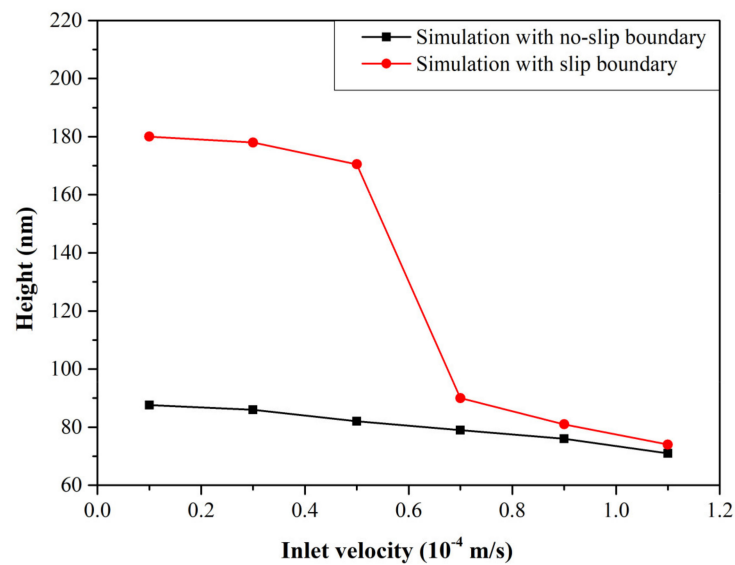


Figure 9. Effect of inlet velocity on the filling height of moth-eye nanostructure.

Figure 10 showed the effect of resin thickness on the filling height of moth-eye nanostructure. As observed, the filling height decreased as the resin thickness increased. It was because the resin thickness was adjusted by the imprinting pressure and smaller resin thickness meant a larger pressure. When the resin thickness became larger, the pressure decreased, and less resin was squeezed into the mold cavity, thereby causing a lower filling height. Besides, it was further found that a larger filling height could be obtained with slip boundary, which was because the slip on the mold caused the resin near the mold side to flow faster than the substrate side, and more resin could be filled into the mold cavity to obtain a larger filling height before the cavity was closed.

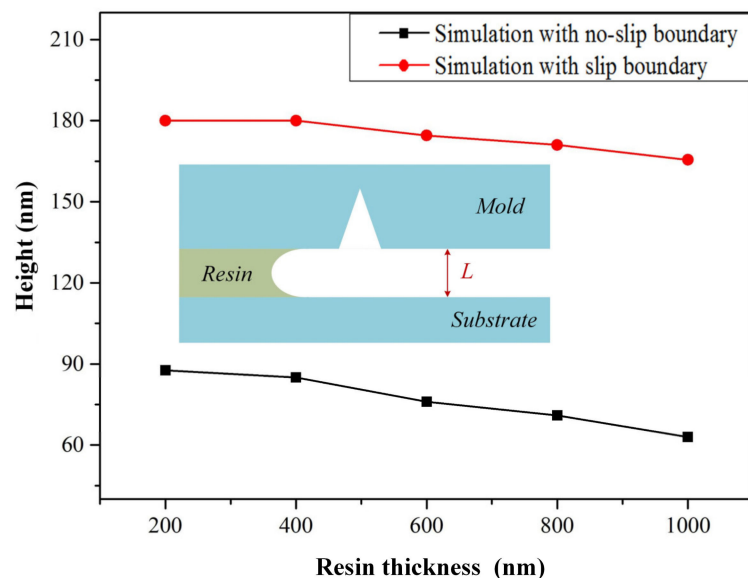


Figure 10. Effect of resin thickness on the filling height of the moth-eye nanostructure.

3.2. Effect of Slip Position

The boundary slip might occur on different positions, substrate side or mold side, and it was difficult to investigate the influence of slip position on filling behavior using the experimental method. Therefore, the effect of slip position on filling behavior was investigated based on the simulation model, as shown in Figure 11. In order to ensure one single variable, the slip speed was set to the same value, which was 2.5×10^{-5} m/s. According to the simulation results, the slip position showed a significant influence on the

resin filling behavior, and the forming height was 87.6 nm, 73.2 nm, 54.3 nm and 180 nm with no-slip on both the mold and the substrate, slip on both the mold and the substrate, slip on the substrate only and slip on the mold only, respectively. Based on the results, it was concluded that the solid–liquid interface property had an important influence on the resin filling process, which affected the slip position.

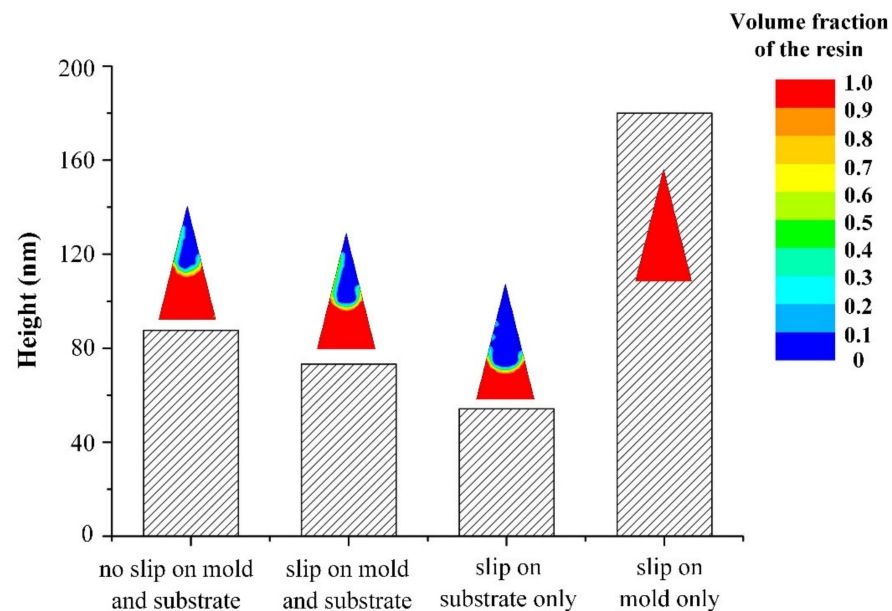


Figure 11. Effect of slip position on the filling height of moth-eye nanostructure.

The resin filling evolution process with different slip positions was further investigated, as shown in Figure 12. It could be found that the resin near the substrate flowed faster when boundary slip occurred on the substrate side only, so the cavity was closed more quickly, thereby lowering the filling height. Besides, it was observed from Figure 12d that the resin near the mold side flowed faster when the boundary slip occurred on the mold side only, and more resin could flow into the mold cavity before the cavity was closed, thereby obtaining a larger filling height.

3.3. Effect of Slip Velocity

Figure 13 showed the effect of slip velocity on the filling height of the moth-eye nanostructure. In order to ensure one single variable, the slip positions were all on the mold side only, the inlet velocity was 1.0×10^{-5} m/s, the resin viscosity was 0.1 Pa·s and the resin thickness was 200 nm, respectively. It could be observed that the filling height increased as the slip velocity increased. However, the influence of slip velocity was not significant when the slip velocity was less than 1.0×10^{-5} m/s, while the filling height was significantly affected when the slip velocity was larger than 1.0×10^{-5} m/s. The reason for this phenomenon was that the filling height was affected by the slip velocity and resin inlet velocity simultaneously, and the filling height was mainly affected by the resin inlet velocity when the slip velocity was small while it was mainly affected by the slip velocity when the slip velocity was larger than a certain threshold [32,33].

Figure 14 showed the filling evolution process with different slip velocity, which was 0 m/s, 1.0×10^{-5} m/s and 2.0×10^{-5} m/s, respectively. It was observed that the flow velocity near the mold side increased as the slip velocity increased so that more resin could flow into the mold cavity under the same conditions, thereby obtaining a larger filling height.

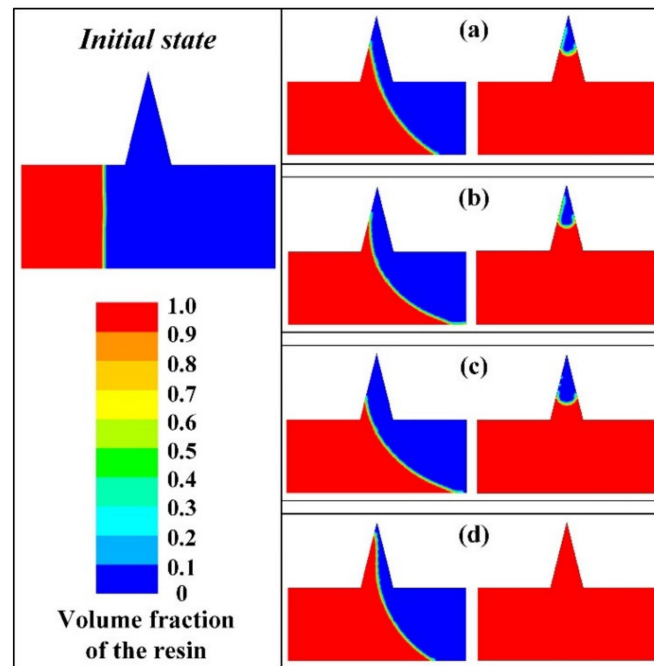


Figure 12. The filling evolution process with different slip positions (a) no-slip on both the mold and the substrate (b) slip on both the mold and the substrate (c) slip on the substrate only (d) slip on the mold only.

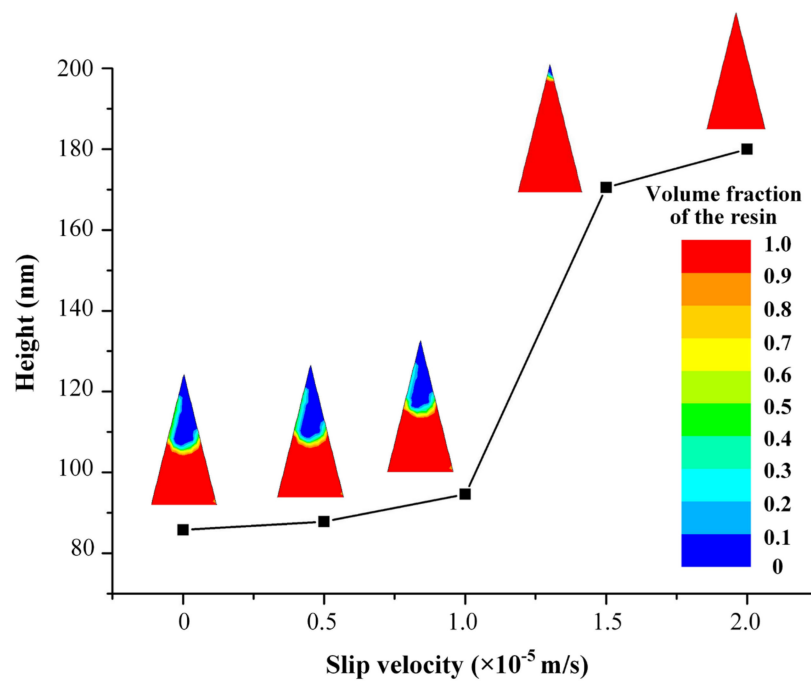


Figure 13. The effect of slip velocity on the filling height of the moth-eye nanostructure.

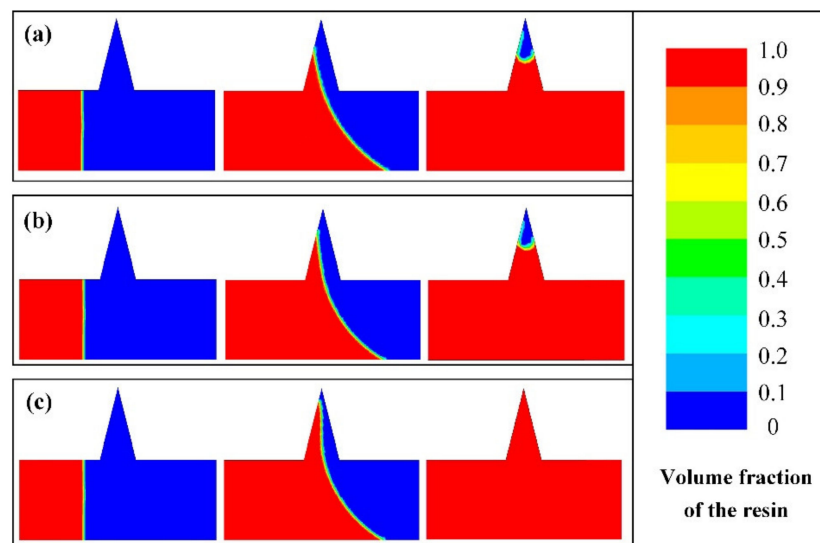


Figure 14. The resin filling evolution process with different slip velocity (a) 0 m/s (b) 1.0×10^{-5} m/s (c) 2.0×10^{-5} m/s.

4. Conclusions

A CFD simulation model was established to investigate the resin filling behavior during the UV-NIL process of the moth-eye nanostructure, where the effect of boundary slip was considered. By comparison with the experimental results, a good consistency was found, indicating that the simulation model could be used to analyze the resin filling behavior in the UV-NIL process of the moth-eye nanostructure.

Based on the proposed model, the effects of process parameters on filling behavior were analyzed, including resin viscosity, inlet velocity and resin thickness. It was found that the inlet velocity showed a more significant effect on filling height than resin viscosity and thickness. Therefore, choosing a reasonable speed was quite important during the UV-NIL of the moth-eye nanostructure, taking into account the forming accuracy and efficiency comprehensively, which could provide guidance for the UV-NIL experiments of the moth-eye nanostructure.

Besides, the effects of boundary conditions on the mold filling behavior of moth-eye nanostructure were also investigated. It was found that the slip position showed a significant influence on the resin filling behavior and the forming height was 87.6 nm, 73.2 nm, 54.3 nm and 180 nm with no-slip on both the mold and the substrate, slip on both the mold and the substrate, slip on the substrate only, and slip on the mold only, respectively. Moreover, the filling height was affected by the slip velocity and resin inlet velocity simultaneously, and the filling height was mainly affected by the inlet velocity when the slip velocity was small while it was mainly affected by the slip velocity when the slip velocity was larger than a certain threshold. The results could provide guidance for the regulation of solid–liquid interface properties.

Author Contributions: Drafting the work, Y.C., X.W.; The acquisition and analysis of data for the work, C.Z., J.W. and Z.S. All authors have read and agreed to the published version of the manuscript.

Funding: This research received no external funding.

Institutional Review Board Statement: Not applicable.

Informed Consent Statement: Not applicable.

Data Availability Statement: Data is contained within the article.

Acknowledgments: The authors would like to thank the Natural Science Foundation of Jiangsu Province (BK20190202), the China Postdoctoral Science Foundation (2021M691926), the Research Project

of State Key Laboratory of Mechanical System and Vibration (MSV202102), the Shandong Provincial Natural Science Foundation (ZR2019BEE062) and Young Scholars Program of Shandong University.

Conflicts of Interest: The authors declare no competing financial interests.

References

1. Chen, H.; Lan, Y.F.; Tsai, C.Y.; Wu, S.T. Low-voltage blue-phase liquid crystal display with diamond-shape electrodes. *Liq. Cryst.* **2016**, *44*, 1124–1130. [[CrossRef](#)]
2. Liu, Y.; Lai, J.; Li, X.; Xiang, Y.; Li, J.; Zhou, J. A quantum dot array for enhanced tricolor liquid-crystal display. *IEEE Photonics J.* **2017**, *9*, 1–7. [[CrossRef](#)]
3. Yoshikawa, K.; Kawasaki, H.; Yoshida, W.; Irie, T.; Konishi, K.; Nakano, K.; Uto, T.; Adachi, D.; Kanematsu, M.; Uzu, H.; et al. Silicon heterojunction solar cell with interdigitated back contacts for a photoconversion efficiency over 26%. *Nat. Energy* **2017**, *2*, 17032. [[CrossRef](#)]
4. Zheng, Z.; Awartani, O.M.; Gautam, B.; Liu, D.; Qin, Y.; Li, W.; Bataller, A.; Gundogdu, K.; Ade, H.; Hou, J. Efficient charge transfer and fine-tuned energy level alignment in a THF-processed fullerene-free organic solar cell with 11.3% efficiency. *Adv. Mater.* **2017**, *29*, 1604241. [[CrossRef](#)] [[PubMed](#)]
5. Goossens, S.; Navickaite, G.; Monasterio, C.; Gupta, S.; Piqueras, J.J.; Pérez, R.; Burwell, G.; Nikitskiy, I.; Lasanta, T.; Galán, T.; et al. Broadband image sensor array based on graphene–CMOS integration. *Nat. Photonics* **2017**, *11*, 366–371. [[CrossRef](#)]
6. Vukusic, P.; Sambles, J.R. Photonic structures in biology. *Nat. Cell Biol.* **2003**, *424*, 852–855. [[CrossRef](#)] [[PubMed](#)]
7. Zhang, C.; Yi, P.; Peng, L.; Ni, J. Optimization and continuous fabrication of moth-eye nanostructure array on flexible polyethylene terephthalate substrate towards broadband antireflection. *Appl. Opt.* **2017**, *56*, 2901–2907. [[CrossRef](#)] [[PubMed](#)]
8. Zhang, C.; Yi, P.; Peng, L.; Lai, X.; Ni, J. Fabrication of moth-eye nanostructure arrays using roll-to-roll uv-nanoimprint lithography with an anodic aluminum oxide mold. *IEEE Trans. Nanotechnol.* **2015**, *14*, 1127–1137. [[CrossRef](#)]
9. Brousseau, E.B.; Dimov, S.S.; Pham, D. Some recent advances in multi-material micro-and nano-manufacturing. *Int. J. Adv. Manuf. Technol.* **2009**, *47*, 161–180. [[CrossRef](#)]
10. Leveder, T.; Landis, S.; Davoust, L.; Chaix, N. Flow property measurements for nanoimprint simulation. *Microelectron. Eng.* **2007**, *84*, 928–931. [[CrossRef](#)]
11. Reddy, S.; Bonnecaze, R.T. Simulation of fluid flow in the step and flash imprint lithography process. *Microelectron. Eng.* **2005**, *82*, 60–70. [[CrossRef](#)]
12. Yanagishita, T.; Kondo, T.; Masuda, H. Preparation of renewable antireflection moth-eye surfaces by nanoimprinting using anodic porous alumina molds. *J. Vac. Sci. Technol. B* **2018**, *36*, 031802. [[CrossRef](#)]
13. Sun, J.; Wang, X.; Wu, J.; Jiang, C.; Shen, J.; Cooper, M.A.; Zheng, X.; Liu, Y.; Yang, Z.; Wu, D. Biomimetic moth-eye nanofabrication: Enhanced antireflection with superior self-cleaning characteristic. *Sci. Rep.* **2018**, *8*, 1–10. [[CrossRef](#)] [[PubMed](#)]
14. Wang, J.; Li, M.; Qiu, J.; Zhou, Y. Filling angle and its effect on filling process in roll-to-roll ultraviolet imprint lithography. *J. Micromech. Microeng.* **2018**, *28*, 035011. [[CrossRef](#)]
15. Jain, A.; Spann, A.; Bonnecaze, R.T. Effect of droplet size, droplet placement, and gas dissolution on throughput and defect rate in UV nanoimprint lithography. *J. Vac. Sci. Technol. B* **2017**, *35*, 011602. [[CrossRef](#)]
16. Kim, K.-D.; Kwon, H.-J.; Choi, D.-G.; Jeong, J.-H.; Lee, E.-S. Resist flow behavior in ultraviolet nanoimprint lithography as a function of contact angle with stamp and substrate. *Jpn. J. Appl. Phys.* **2008**, *47*, 8648–8651. [[CrossRef](#)]
17. Peng, L.; Yi, P.; Wu, H.; Lai, X. Study on bubble defects in roll-to-roll UV imprinting process for micropillar arrays II: Numerical study. *J. Vac. Sci. Technol. B* **2016**, *34*, 051203. [[CrossRef](#)]
18. Wu, H.; Yi, P.; Peng, L.; Lai, X. Study on bubble defects in roll-to-roll UV imprinting process for micropillar arrays. I. Experiments. *J. Vac. Sci. Technol. B* **2016**, *34*, 021201. [[CrossRef](#)]
19. Tian, H.; Shao, J.; Ding, Y.; Li, X.; Li, X. Numerical studies of electrically induced pattern formation by coupling liquid dielectrophoresis and two-phase flow. *Electrophoresis* **2011**, *32*, 2245–2252. [[CrossRef](#)] [[PubMed](#)]
20. Nagaoka, Y.; Suzuki, R.; Hiroshima, H.; Nishikura, N.; Kawata, H.; Yamazaki, N.; Iwasaki, T.; Hirai, Y. Simulation of resist filling properties under condensable gas ambient in ultraviolet nanoimprint lithography. *Jpn. J. Appl. Phys.* **2012**, *51*, 06FJ07. [[CrossRef](#)]
21. Shibata, M.; Horiba, A.; Nagaoka, Y.; Kawata, H.; Yasuda, M.; Hirai, Y. Process-simulation system for UV-nanoimprint lithography. *J. Vac. Sci. Technol. B* **2010**, *28*, C6M108. [[CrossRef](#)]
22. Ye, H.; Zhang, Q.; Shen, L.; Li, M. Bubble defect control in low-cost roll-to-roll ultraviolet imprint lithography. *Micro Nano Lett.* **2014**, *9*, 28–30. [[CrossRef](#)]
23. Ali, J.; Kim, H.; Cheang, U.K.; Kim, M.J. Micro-PIV measurements of flows induced by rotating microparticles near a boundary. *Microfluid. Nanofluid.* **2016**, *20*, 131. [[CrossRef](#)]
24. Cross, B.; Barraud, C.; Picard, C.; Léger, L.; Restagno, F.; Charlaix, É. Wall slip of complex fluids: Interfacial friction versus slip length. *Phys. Rev. Fluids* **2018**, *3*, 062001. [[CrossRef](#)]
25. Morihara, D.; Nagaoka, Y.; Hiroshima, H.; Hirai, Y. Numerical study on bubble trapping in UV nanoimprint lithography. *J. Vac. Sci. Technol. B* **2009**, *27*, 2866. [[CrossRef](#)]
26. Jain, A.; Bonnecaze, R.T. Fluid management in roll-to-roll nanoimprint lithography. *J. Appl. Phys.* **2013**, *113*, 234511. [[CrossRef](#)]
27. Zhang, C.; Zhu, Y.; Yi, P.; Peng, L.; Lai, X. Fabrication of flexible silver nanowire conductive films and transmittance improvement based on moth-eye nanostructure array. *J. Micromech. Microeng.* **2017**, *27*, 075010. [[CrossRef](#)]

28. Rashidi, S.; Akar, S.; Bovand, M.; Ellahi, R. Volume of fluid model to simulate the nanofluid flow and entropy generation in a single slope solar still. *Renew. Energy* **2018**, *115*, 400–410. [[CrossRef](#)]
29. Wu, W.; Hu, C.; Hu, J.; Yuan, S.; Zhang, R. Jet cooling characteristics for ball bearings using the VOF multiphase model. *Int. J. Therm. Sci.* **2017**, *116*, 150–158. [[CrossRef](#)]
30. Hiroshima, H.; Suzuki, K. Study on change in UV nanoimprint pattern by altering shrinkage of UV curable resin. *Jpn. J. Appl. Phys.* **2011**, *50*, 06GK09. [[CrossRef](#)]
31. Horiba, A.; Yasuda, M.; Kawata, H.; Okada, M.; Matsui, S.; Hirai, Y. Impact of resist shrinkage and its correction in nanoimprint lithography. *Jpn. J. Appl. Phys.* **2012**, *51*, 06FJ06. [[CrossRef](#)]
32. Donggang, Y.; Byung, K. Simulation of the filling process in micro channels for polymeric materials. *J. Micromech. Microeng.* **2002**, *12*, 604.
33. Arabpour, A.; Karimipour, A.; Toghraie, D. The study of heat transfer and laminar flow of kerosene/multi-walled carbon nanotubes (MWCNTs) nanofluid in the microchannel heat sink with slip boundary condition. *J. Therm. Anal. Calorim.* **2017**, *131*, 1553–1566. [[CrossRef](#)]